LBL-25914
Preprint

Lawrence Berkeley Laboratory
UNIVERSITY OF CALIFORNIA

Materials & Chemical
Sciences Division

LABORATORY
DEC 6 1988

Submitted to Journal of Applied Physics

Domain Structure and Microstructure of Co-Ni Oblique Incidence Thin Films

H.-M. Ho, G.J.-S. Gau, and G. Thomas

September 1988

TWO-WEEK LOAN COPY
This is a Library Circulating Copy
which may be borrowed for two weeks.

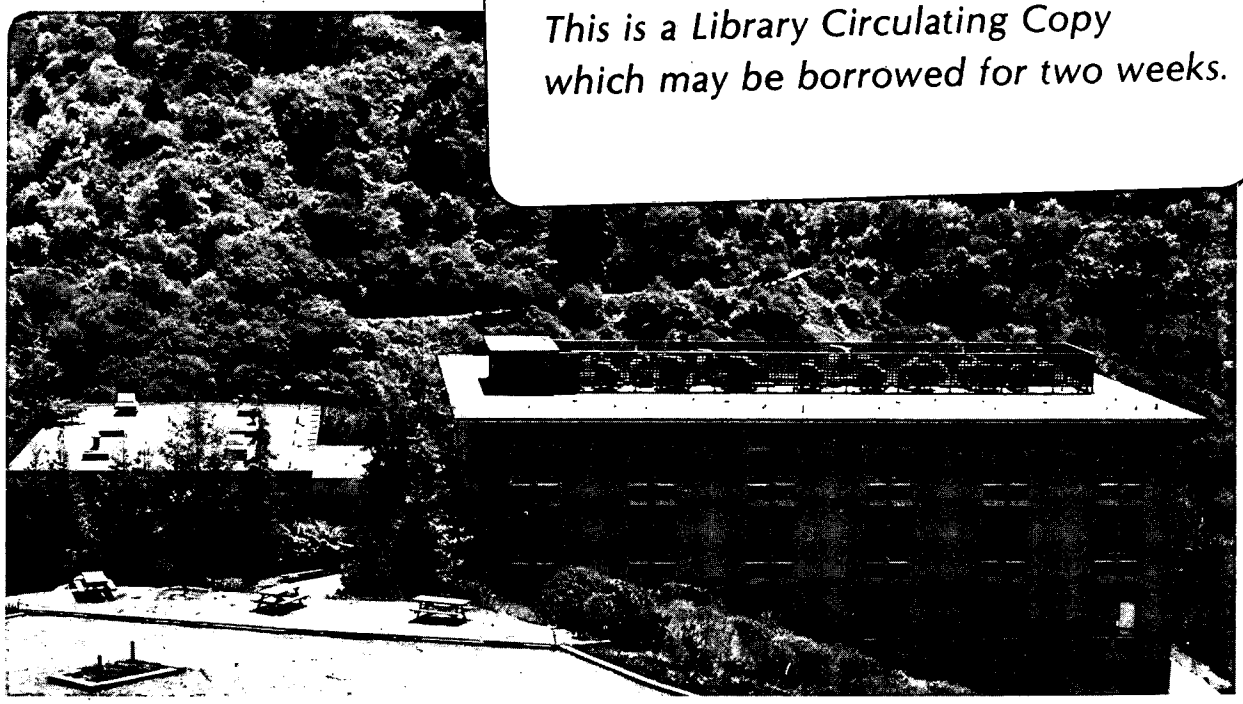

Prepared for the U.S. Department of Energy under Contract Number DE-AC03-76SF00098.

LBL-25914

DISCLAIMER

This document was prepared as an account of work sponsored by the United States Government. While this document is believed to contain correct information, neither the United States Government nor any agency thereof, nor the Regents of the University of California, nor any of their employees, makes any warranty, express or implied, or assumes any legal responsibility for the accuracy, completeness, or usefulness of any information, apparatus, product, or process disclosed, or represents that its use would not infringe privately owned rights. Reference herein to any specific commercial product, process, or service by its trade name, trademark, manufacturer, or otherwise, does not necessarily constitute or imply its endorsement, recommendation, or favoring by the United States Government or any agency thereof, or the Regents of the University of California. The views and opinions of authors expressed herein do not necessarily state or reflect those of the United States Government or any agency thereof or the Regents of the University of California.

LBL-25914

Domain Structure and Microstructure of Co-Ni Oblique Incidence Thin Films

Huei-Min Ho*, George J.-S. Gau**, and Garth Thomas*

*Department of Materials Science and Mineral Engineering
University of California
and
Materials and Chemical Sciences Division
Lawrence Berkeley Laboratory
1 Cyclotron Road
Berkeley, California 94720

**MPI, Control Data Corporation
Minneapolis, MN 55435

September 1988

Domain structure and microstructure of Co-Ni oblique incidence thin films

Huei-Min Ho*, George J. -S. Gau**, and Gareth Thomas*

*Department of Materials Science and Mineral Engineering, Materials and Chemical Sciences Division, Lawrence Berkeley Laboratory, University of California, Berkeley, CA 94720

**MPI, Control Data Corporation, Minneapolis, MN 55435

Abstract

The magnetic properties of thin films produced by vacuum evaporation depend on the deposition conditions, such as incident angle(α) and substrate temperature. These effects have been investigated in CoNi oblique incidence thin films by transmission electron microscopy. Both incident angle and substrate temperature are observed to have significant effects on the magnetization easy direction in the films. Low angle films($\alpha \leq 60°$) are magnetically continuous with in-plane easy axes and reverse their magnetization by domain wall motion. On the contrary, high angle films are magnetically isolated with an out-of-plane easy axis and reverse their magnetization by an incoherent rotation process.

Microstructural results show that a c-axis texture increases with increasing incident angle. In high angle films, the columns are single crystals and have a high defect density. The c axis of the columns does not coincide with the column axis. Thus, it is concluded that the origin

of the magnetic anisotropy in low angle films is mainly due to shape anisotropy. On the other hand, in high angle films, crystalline anisotropy and stress anisotropy should be taken into account in addition to the shape anisotropy.

INTRODUCTION

For high density recording tape applications, the oblique-incidence deposition technique, which induces magnetic anisotropy by controlling the angle of incidence of the vapor flux with respect to the substrate normal, has being extensively studied[1,2,3]. In such a process, the magnetic properties of deposited thin films are very sensitive to the deposition conditions, e.g., by modifying the angle of incidence and substrate temperature, a film of a given composition can be made to be isotropic or anisotropic, of low or high coercivity, of parallel or transverse in-plane easy axis.

The angle of incidence has been reported to have the following effects: 1. direction of easy axis, which was found[3,4,5] to switch from perpendicular (to the in-plane projected incident direction) in low angle films to parallel in high angle films at a critical angle of 60°, 2. columnar diameter, which was reported by Speliotis et. al.[6] to increase from 20~30Å at normal incident to 80~100Å at 65° and about 1000Å at 75° and by Ozawa et. al.[7] to increase with the film thickness, and 3. coercivity, which was observed to increase drastically from around 100 Oe in low angle films to >1000 Oe in high angle films[6,8,9]. In addition, the substrate temperature has been reported by Kondorsky and Denisov[10] to have significant effects on the direction of the in-plane easy axis in the thin films.

It is known that thin film properties are related to morphology, microstructure, domain structure, and magnetization reversal mechanism. However, with regard to oblique-incidence films, these relationships are not yet precisely known. Therefore, the present study was undertaken to investigate in obliquely deposited CoNi films, the

effects of incident angle and substrate temperature on the coercivity, squareness ratio, magnetic domain structure and microstructure. The latter were characterized by transmission electron microscopy, including Lorentz imaging and convergent beam diffraction. Magnetization reversal mechanisms in the oblique incidence films were also studied by rotational hysteresis analysis.

EXPERIMENT

Thin films investigated in this study were deposited by electron-beam evaporation from an alloy slug with a Co-20at%Ni nominal composition onto plastic films (Kapton) and carbon coated mica at various oblique incidence angles (α), where α is the angle between the incident vapor direction and the substrate normal. The angles ranged from 40° to 85°. The incident plane, which will be frequently referred to in the text, is defined also by the incident vapor direction and the substrate normal. These parameters are illustrated in Fig. 1.

The deposition conditions include: a deposition rate of 10~15 Å/s, a base pressure during deposition on the order of 1~2 $x10^{-5}$ Torr, and a source to substrate distance of 50cm. The substrate temperatures (Ts) used were room temperature (RT) and 250°C. Throughout this paper, thin films will be specified by the two parameters studied: substrate temperature and incident angle, e.g., 40°, 250°C film, or 85°, RT film. Static magnetic properties were measured using a vibrating sample magnetometer(VSM) with an applied field of 10 KOe. Rotational hysteresis was measured as a function of the applied magnetic field in

the film plane using a torque magnetometer.

Transmission electron microscopy, including Lorentz microscopy and convergent beam diffraction, was performed using a 100KV Philips 400 microscope. Films were prepared by two methods for transmission electron microscopy, namely, ion-milling for plan-view specimens and ultramicrotomy for cross-section specimens.

EXPERIMENTAL RESULTS

In Fig. 2, the squareness ratios(S, measured both parallel and perpendicular to the incident plane) of the Co-20Ni thin films of constant thickness(~1500Å) are plotted against the angle of incidence. In 250°C films, S has higher values (around 0.9) along the perpendicular and parallel directions in 40°, and in 75° and higher angles, respectively, with a cross-over at 60°. In RT films, S has a higher value (also around 0.9) along the parallel direction in all films. Fig. 3 shows the coercivity (also measured both parallel and perpendicular to the incident plane) of these oblique incidence films as a function of incident angle. It is clearly seen that high angle($\alpha > 60°$) and low Ts(RT) films have much higher coercivity values than those of low angle($\alpha \leq 60°$) and high Ts(250°C) films.

In order to understand the origin of these magnetic properties, the structure of the films was characterized using various methods of electron microscopy and diffraction. The results of Lorentz microscopy on the oblique incidence films are shown in Fig. 4. Lorentz microscopy reveals magnetic domain structures in two ways: Fresnel imaging(Figs. 4a and c), which uses an under-focusing method to image domain walls

as dark or white lines, and Foucault imaging (Figs. 4b and d), which utilizes a displaced-aperture method to obtain diffraction contrast in the domains which then appear as dark or white regions. As shown in Fig. 4a, the 40°, 250°C film has very large magnetic domains with their easy directions lying perpendicular to the incident plane. The sizes of the domains are of the order of several tens of microns and the reverse domains seen in Fig. 4a are edge domains formed in an effort to reduce the magnetostatic energy of the film. In Fig. 4b, the 60°, 250°C film consists of two sets of elongated domains crossing each other. The averaged long axis directions of the domains, which are also the easy directions, are approximately parallel and perpendicular, respectively, to the projected incident vapor direction (Fig.1). In figure 4c, which shows elongated domains in both 40°, RT, and 60°, RT films, the averaged long axis direction is observed to lie along the projected incident direction. These results indicate that in low angle films($\alpha \leq 60°$), the easy axes of the oblique incidence films change from perpendicular (to the incidence plane) at 40°, 250°C, to biaxial(in-plane) at 60°, 250°C, and to parallel at 40° and 60°, RT. These domain structures and images of cross-tie walls(arrowed, Fig. 4c) reveal that the corresponding films are magnetically continuous, i.e., exchange interaction occurs between the grains.

In contrast to low angle films, no domain structure has ever been observed in high angle films(75°and 85°, both RT and 250°C), as shown in Fig. 4d (the observed contrast is non-magnetic, amplitude contrast due to the columnar grain and high porosity of the films). However, as shown in Fig. 5a, stray fields(arrowed) can be seen around the high

angle films viewed in plan. These stray fields, which when imaged in the Foucault mode, show dark and white contrast due to the reversed directions of flux lines near the film edges, as is also shown in Fig. 5b. Fig. 5b is an 85°, RT sample thinned from the substrate side and appears as chains of clusters due to the particle-like structure of the film. Although these stray field images may not represent the actual sizes of the smallest magnetic clusters due to magnetostatic interaction in as-deposited films, they nevertheless indicate the dimensions of the order of tenths of a micron.

The microstructure of a 40°, 250°C film is shown in Fig. 6. The film is observed to have a chain-like morphology(Fig. 6b) with averaged direction perpendicular to the incident plane and to have a hexagonal close packed (hcp) structure with no preferred crystallographic directions(Fig. 6a). The electron diffraction pattern and several other diffraction rings that appear in other films(e.g., Fig. 10) are illustrated and indexed in Fig. 7. These data suggest that the magnetic anisotropy(Fig. 6c) in the film is mainly due to the shape anisotropy of the chain-like morphology.

However, in contrast to the 40°, 250°C film, the morphologies of the rest of the films (including 60° and higher angle, 250°C films and all RT films) show a canted columnar structure with columns growing toward the incident direction(Fig. 8). In a 60°, 250°C film, the columnar structure viewed in plan is shown in Fig. 9a; in addition, a weak c-axis texture, as manifested by the slight arcing in the 0002 ring in Fig. 9b, is observed. Two sets of magnetic domains crossing each other can be seen in the Foucault images of Figs. 8c and d, in which the arrows indicate opposite magnetic contrast, suggesting that

both shape anisotropy due to the chain-like morphology and magnetic anisotropy due to the columnar morphology and weak c-axis texture operate together.

The canted columnar structure is clearly shown in Fig. 8 for various RT films: (a), (b), and (c) are 40°, 60°, and 75° films of similar thickness (~1500Å), respectively, and (d) is an 85° film of ~3000Å thick. The angle of the canted columnar structure(i.e., column axis direction, β) is observed to increase with increasing incident angle. However, the tangent rule: $\tan \alpha = 2 \tan \beta$[11], which has been used to describe the relation of the incident angle and the column axis direction, is not followed by these films. The columnar diameter is about 100Å in all films regardless of the incident angle and the film thickness, and the aspect ratio of the columns can be as high as 60, as in a 1500Å thick 75° film(Fig. 8c).

High angle films are observed to have a porous structure which enables one to examine the columns individually in a cross-section specimen. Convergent beam diffraction and dark field imaging techniques employed on such specimens show that the columns are single crystals with a very high fault defect density on the basal planes, as shown in Fig. 11 for an 85°, 250°C sample.

The selected area diffraction patterns of the RT films viewed in plan are shown in Fig. 10. It is clearly seen from these results that the c-axis texture increases with increasing incident angle, as the arcing in 0002 rings becomes more evident with increasing incident angle. Furthermore, the arced pairs of the 0002 rings are oriented along the projected incident vapor directions in the film planes. The porous

Furthermore, the arced pairs of the 0002 rings are oriented along the projected incident vapor directions in the film planes. The porous structure of the high angle films is also verified by the diffraction patterns, as CoO rings become evident in Fig. 10c and d, suggesting there may be physical separation of the columns which allows CoO to form and grow between them. In addition, a faint ring which can be indexed as face-centered cubic(fcc) {200} can also be observed in the diffraction patterns.

In contrast to the uniform columnar diameter observed in RT films, columns with a conical shape, similar to those reported by Ozawa et.al.[7] on iron films, are observed in an 85°, 250°C film(Fig. 11a). The columnar diameter in such films ranges from 100Å to 1000Å. Convergent electron beam diffraction(Fig. 11d) probed along the column at positions marked 1, 2, 3, and 4, and dark field imaging(Fig. 11b) show that the entire column must remain as a single crystal even at 4000Å in length. However, the c axis of the column, which is normal to the fault planes as shown in Fig. 11b and c, is not aligned with the column axis.

The fringe contrast parallel to the trace of the (0001) basal planes (e.g., Fig. 11b) is frequently observed in evaporated and sputtered films, and is probably due to growth faults formed during deposition. In Fig. 11c, the variation in the intensity of diffraction spots, and the appearence of forbidden reflections such as (0001), are consistent with such an interpretation. Such faults can change the ABAB hcp stacking to ABCABC fcc stacking, and can account for the faint fcc ring in Fig. 10.

DISCUSSION

The observed variation in squareness ratio reflects the change of magnetization easy axis, from perpendicular to the incident plane, to biaxial and then to parallel to the incident plane. Bearing in mind that the incident angle contributes to directional mobility[12] so that adatoms move preferentially along the projected direction of the incident vapor direction, and that substrate temperature contributes to random mobility, then the magnetic switching phenomenon simply reflects the competition between the two processing parameters. Thus, in the 40°, 250°C film, the mobility due to the higher substrate temperature predominates so that the adatoms at nuclei tend to diffuse randomly to form a spherical shape in order to reduce surface energy. The film then develops into a chain-like structure due to a self-shadowing mechanism, as first proposed by Smith et.al.[13], and is observed in many other low angle films[14]. In the 60°, 250°C film, while the effect of the chain-like morphology remains visible, i.e., domains have their long axis perpendicular to the incident plane, the directional mobility due to the higher incident angle facilitates growth of the columnar structure with the development of a c-axis texture. Such a process will induce another set of domains to be oriented with their long axis parallel to the incident plane. The observed biaxial anisotropy suggests that the effects due to incident angle and substrate temperature are balanced with each other. In the 75° and 85°, 250°C films and all RT films, the directional mobility of atoms arising from the incident angle effect predominates, and therefore, only the anisotropy parallel to the incident plane is observed.

It is important to note that these results indicate that the

incident angle is not solely responsible for the switching phenomenon as reported by several authors[3,4], but is affected rather significantly by the substrate temperature as reported by Kondorsky and Denisov[10].

The in-plane magnetic domain structures and the similar low coercivity (~100 Oe) measured along both parallel and perpendicular directions in the low angle films indicate that the films are magnetically continuous. Although the magnetic domain structure varies in these low angle films, the magnetization reversal may take place by a common mechanism, namely, domain wall motion. The observed weak or no c-axis texture in the low angle films suggests that magnetic anisotropy is primarily due to the shape anisotropy, either as a result of the chain-like morphology(in 40°, 250°C film) or of the columnar morphology(in RT films).

In high angle films, however, stray fields(Fig. 5) imply that the columns behave like single domain particles and interact with each other to form small cluster units(like small magnets), and they give rise to the observed stray fields. The stray field, the high coercivity, and the CoO rings all suggest that the films have a magnetically isolated structure. In order to elucidate the possible coercivity mechanism, rotational hysteresis analysis was undertaken[15]. The rotational hysteresis integrals R_H obtained, indicate that the reversal mechanism is by an incoherent rotation process which also supports the observations that the films have a magnetically isolated structure.

If the faults in the high angle films are growth faults, they can be characterized by a c axis or component of this displacement vector equivalent to a stress axis. In this case, such a stress anisotropy may

add to the crystal anisotropy. The observed single crystal structure of the columns, their c-axis texture, and high (0001) fault density show that besides the shape anisotropy due to the large aspect ratio of the columns, the crystalline anisotropy(c-axis texture) and stress anisotropy(high defect density) may all contribute significantly to the total anisotropy. Hence, the columns should possess a mixed anisotropy with the easy axis lying between the c-axis direction and the column axis direction. Indeed, this out-of-plane easy axis has been observed from the results of angular variation of coercivity measurements[16].

Since the conical-shaped columns cannot be examined by Lorentz microscopy, because Lorentz microscopy can only be done with the objective lens turned off and thus sacrifices spatial resolution, the differences in coercivity between the RT and the 250°C high angle films cannot be explained in terms of defects and conical shape. However, a higher substrate temperature generally increases the dispersion of the column axis direction with respect to the incident vapor direction, because of the higher random atomic mobility. Since a dispersion in the column axis direction represents a dispersion in the easy axis direction, a lower value of coercivity can be expected from a higher degree of easy axis dispersion in 250°C films.

SUMMARY

The magnetization easy axes in oblique incidence Co-20Ni thin films are observed to vary with incident angle and substrate temperature. A high incident angle contributes to an easy axis parallel to the incident plane, whereas a high substrate temperature contributes to an easy axis perpendicular to the incident plane. Low

angle films($\alpha \leq 60°$) are magnetically continuous with in-plane easy axes and, in spite of the differences in the domain structures, may reverse their magnetization by domain wall motion. On the contrary, high angle films(75° and 85°) are magnetically isolated with an out-of-plane easy axis. Rotational hysteresis analysis indicates that the reversal mechanism in high angle films is by an incoherent rotation process.

Microstructural results show that c-axis texture increases with increasing incident angle and is oriented along the projected incident vapor direction. In high angle films, the columns are single crystals and have a high fault density; the c axis of the columns does not coincide with the column axis.

The origin of the magnetic anisotropy in small angle films is mainly due to the shape anisotropy. On the other hand, in high angle films, the crystalline anisotropy due to a c-axis texture and the stress anisotropy due to the high stacking fault density should be taken into account in addition to the shape anisotropy.

ACKNOWLEDGEMENTS

This work was mainly supported by the Director, Office of Energy Research, Office of Basic Energy Sciences, Materials Science Division of the U.S. Department of Energy under contract No. DE-AC03-76SF00098. Domain structure observation was done when HMH was supported by the National Science Foundation under contract No. DMR-8707241E. Thin film deposition was done when JSG was with Eastman Kodak company.

REFERENCES

[1] T. C. Arnoldussen, E. M. Rossi, A. Ting, A. Brunsch, J. Schneider, and G. Trippel, IEEE Trans. Magn., **Mag-20**, 821 (1984).

[2] T. Tanaka, K. Yazawa, and H. Masuya, IEEE Trans. Magn., **Mag-21**, 2090 (1985).

[3] E. Kita, K. Tagawa, M. Kamikubota, and A. Tasaki, IEEE Trans. Magn., **Mag-17**, 3193 (1981).

[4] S. L. Zeder, J.-F. Silvain, M. E. Re, M. H. Kryder and C. L. Bauer, J. Appl. Phys., **61**, 3804 (1987).

[5] M. S. Cohen, J. Appl. Phys., **32**, 87S (1961).

[6] D. E. Speliotis, G. Bate, J. K. Alstad, and J. R. Morrison, J. Appl. Phys., **36**, 972 (1965).

[7] K. Ozawa, H. Masuya, and M. Takahashi, J. Magn. Magn. Mat., **40**, 175 (1983).

[8] T. Tanaka, T. Miyazaki, E. Kita, and A. Tasaki, IEEE Trans. Magn., **Mag-19**, 1650 (1983).

[9] J. R. Morrison, Electrochem. Tech., **6**, 419 (1968).

[10] E. I. Kondorsky and P. P. Denisov, IEEE Trans. Magn., **Mag-6**,167 (1970).

[11] J. M. Nieuwenhuizen and H. B. Haarnstra, Philips Tech. Rev. **27**, 87 (1966).

[12] J. G. W. Van de Waterbeemd and G. W. Van Oosterhout, Philips Res. Rep., **22**, 375 (1967).

[13] D. O. Smith, J. Appl. Phys., **30**, 264S (1959).

[14] Y. J. Wang, Q. Tang, Zh. Q. Wang, H. J. Fan, S. Y. Fan, and F. H. Li, J. Magn. Magn. Mat., **51**, 315 (1985).

[15] J. -S. Gau, H. -M. Ho, and G. Thomas, presented at the 4th Joint MMM-Intermag Conference, Vancouver, Canada, July 12-15, 1988.

[16] J. S. Gau and C. F. Brucker, J. Appl. Phys., **57**, 3988 (1985).

FIGURE CAPTIONS

Fig. 1 Illustration of technical terms related to oblique-incidence deposition.

Fig. 2 The squareness ratio of the 250°C films(a) and the RT films(b) plotted as a function of incident angle.

Fig. 3 The coercivity of the 250°C films(a) and the RT films(b) plotted as a function of incident angle.

Fig. 4 Magnetic domain structures of oblique incidence films; preparation conditions are specified in each micrograph. I.D. is for projected incident vapor direction. Arrows depict the magnetization directions in the films, see text.

Fig. 5 Foucault images of a 75°, RT film(a) and an 85°, RT film(b), showing stray fields(arrowed) around the films. These stray fields indicate that the columns in high angle films behave like single domain particles.

Fig. 6 Diffraction pattern(a), bright field image(b), and Fresnel image (c), of a 40°, 250°C film, showing no c-axis texture, a chain-like morphology and magnetic anisotropy perpendicular to the incident plane. Arrows in (c) indicate magnetization directions.

Fig. 7 Schematic illustration of electron diffraction rings(a) commonly observed in the Co-Ni specimens, and (b) their corresponding indices.

Fig. 8 Bright field images of cross-section samples of thin films deposited at 40°(a), 60°(b), 75°(c), and 85°(d). The column axis direction is observed to increase with increasing incident angle.

Fig. 9 Bright field image(a), diffraction pattern(b), Foucault images (c and d) of a 60°, 250°C film, showing biaxial anisotropy.

Fig. 10 Diffraction patterns of the RT films in Fig. 7 viewed in plan. The c-axis texture increases with increasing incident angle.

Fig. 11 Bright field image of an 85°, 250°C film(a), showing columns with a conical shape; dark field image of such a column with conical shape(b), and convergent beam diffraction(c and d) of the column in (b), showing that the column is a single crystal, stacking faults on {0001} and the column axis is not aligned to the c axis direction.

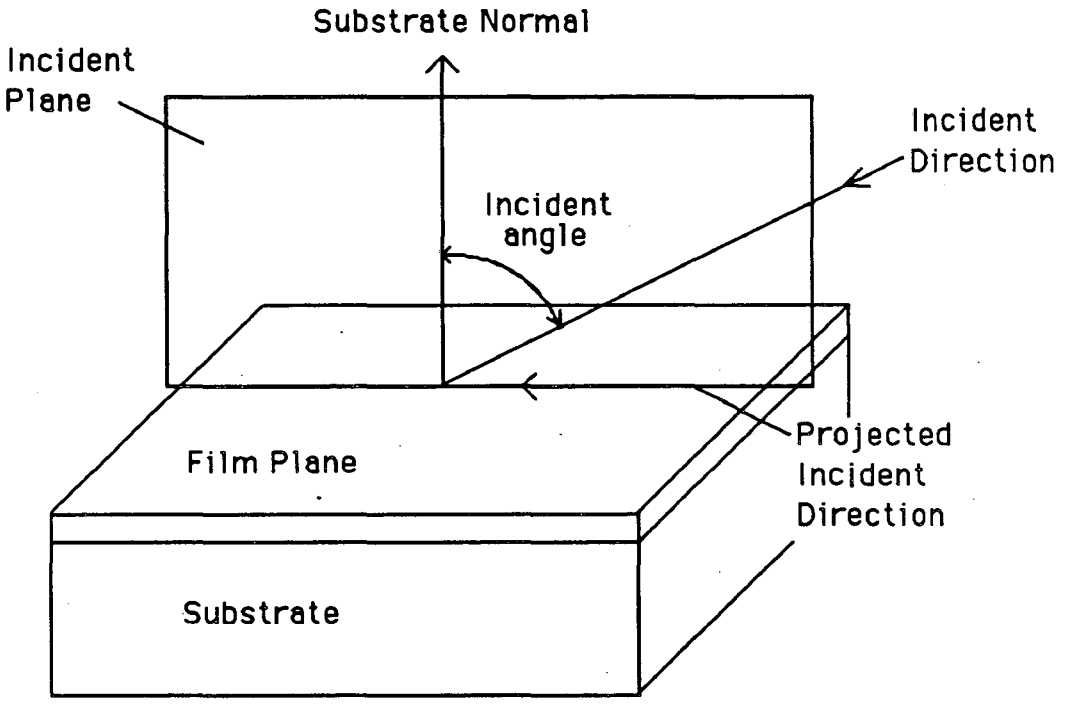
Substrate Normal
Incident
Plane
Incident
Direction
Incident
angle
Film Plane
Projected
Incident
Direction
Substrate

XBL 883-1038

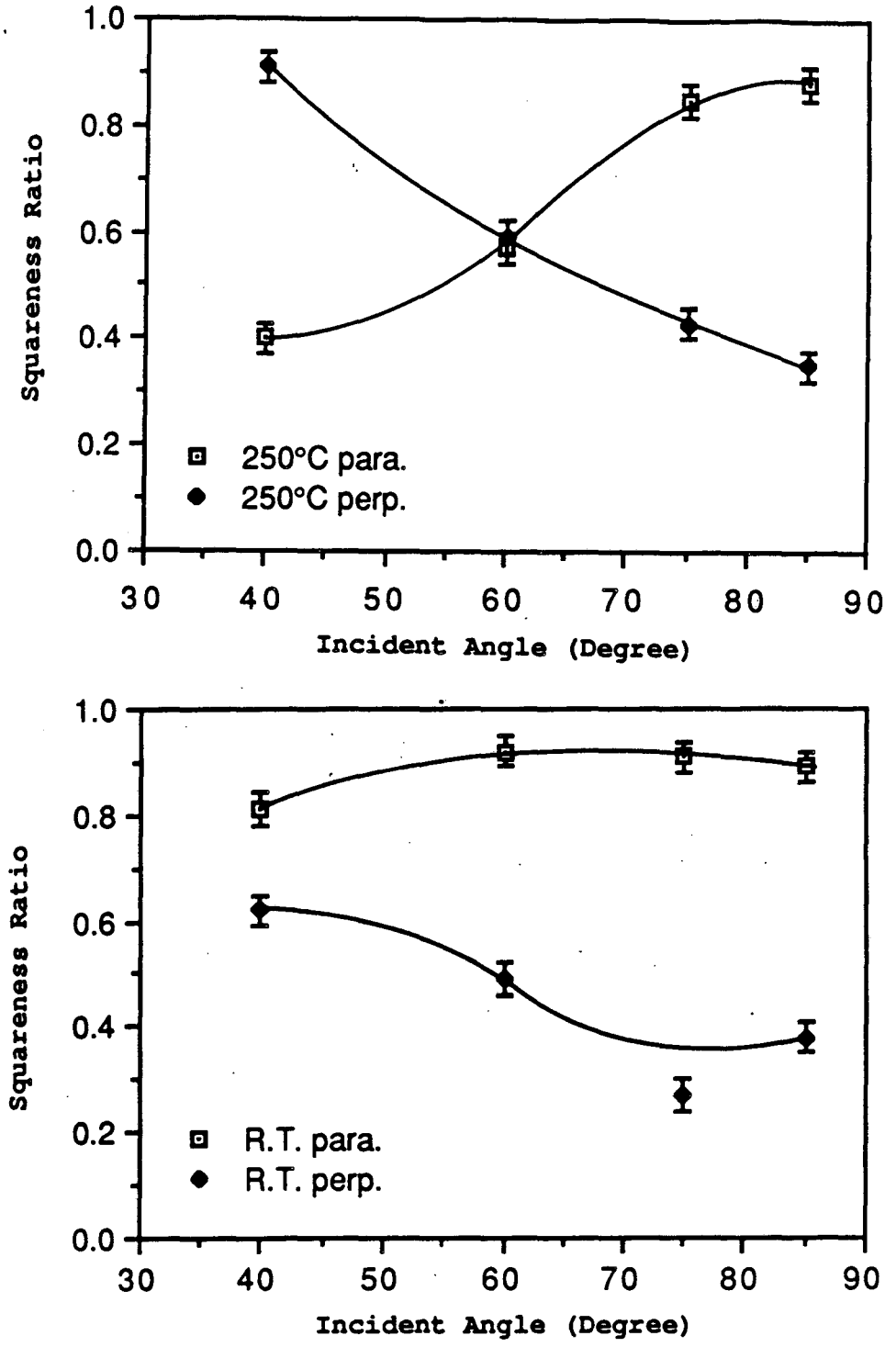
1.0
0.8
0.6
0.4
0.2
0.0
Squareness Ratio
250°C para.
250°C perp.
30
40
50
60
70
80
90
Incident Angle (Degree)
1.0
0.8
0.6
0.4
0.2
0.0
Squareness Ratio
R.T. para.
R.T. perp.
30
40
50
60
70
80
90
Incident Angle (Degree)

XBL 883-1039

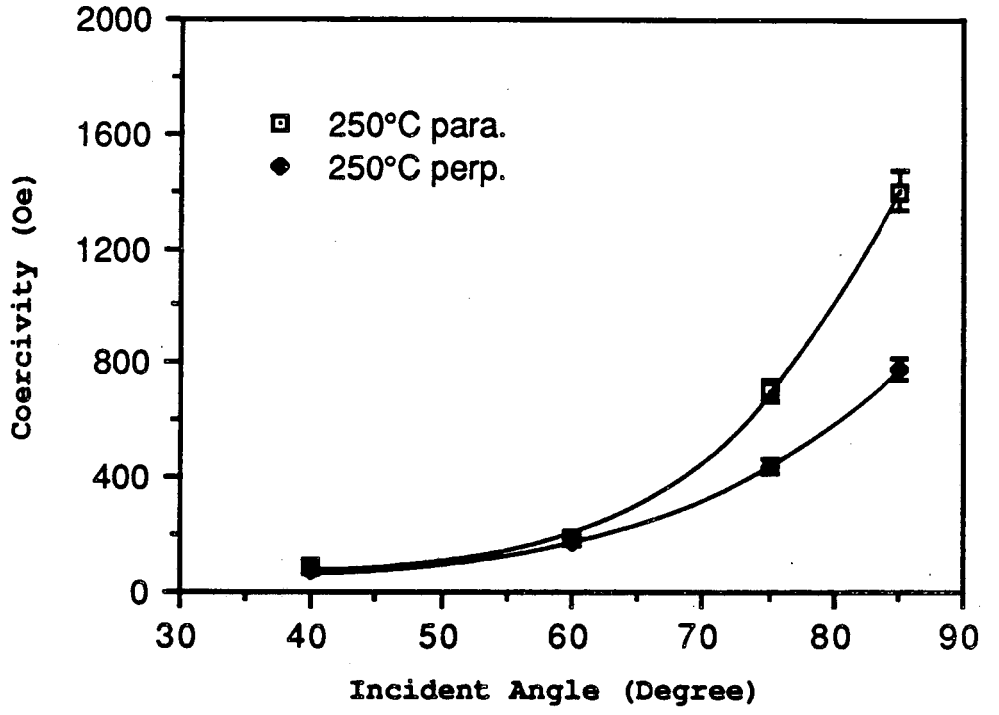
2000
1600
1200
800
400
0
Coercivity (Oe)
250°C para.
250°C perp.
30
40
50
60
70
80
90
Incident Angle (Degree)

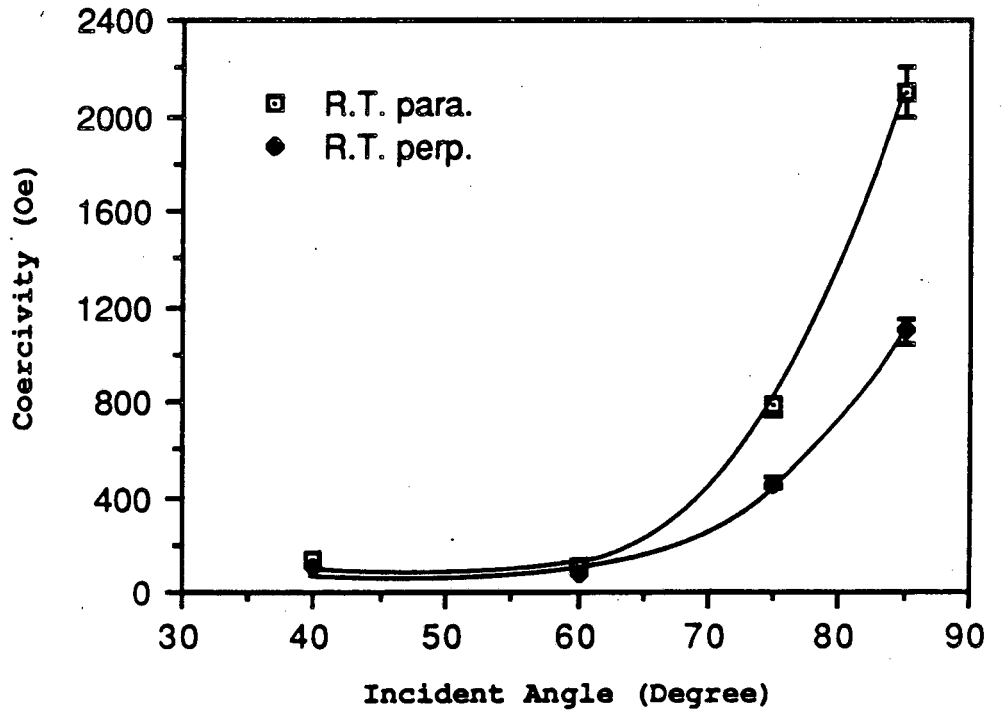
2400
2000
1600
1200
800
400
0
Coercivity (Oe)
R.T. para.
R.T. perp.
30
40
50
60
70
80
90
Incident Angle (Degree)

XBL 883-1040

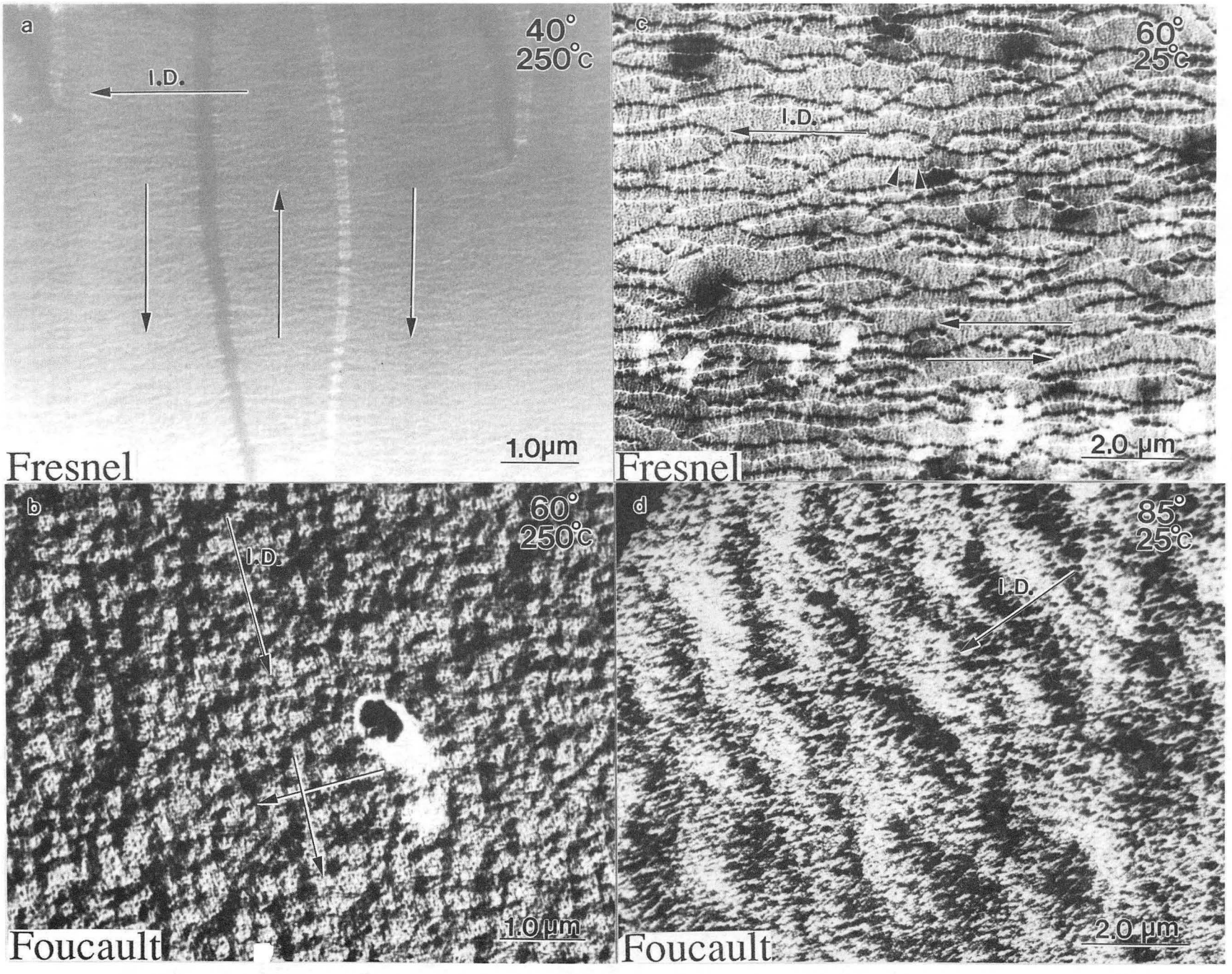

XBB 881-704A

21

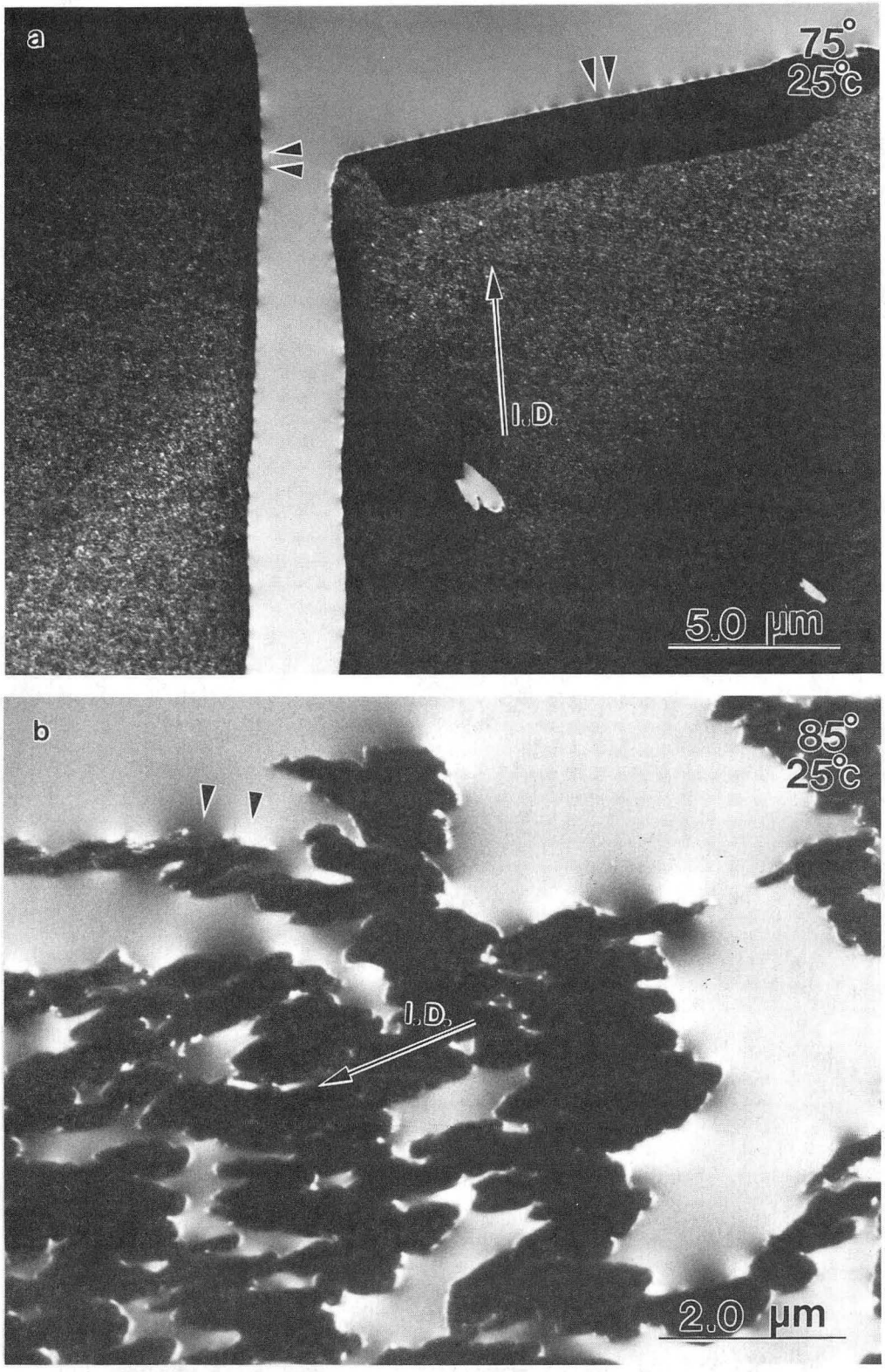

XBB 881-705A

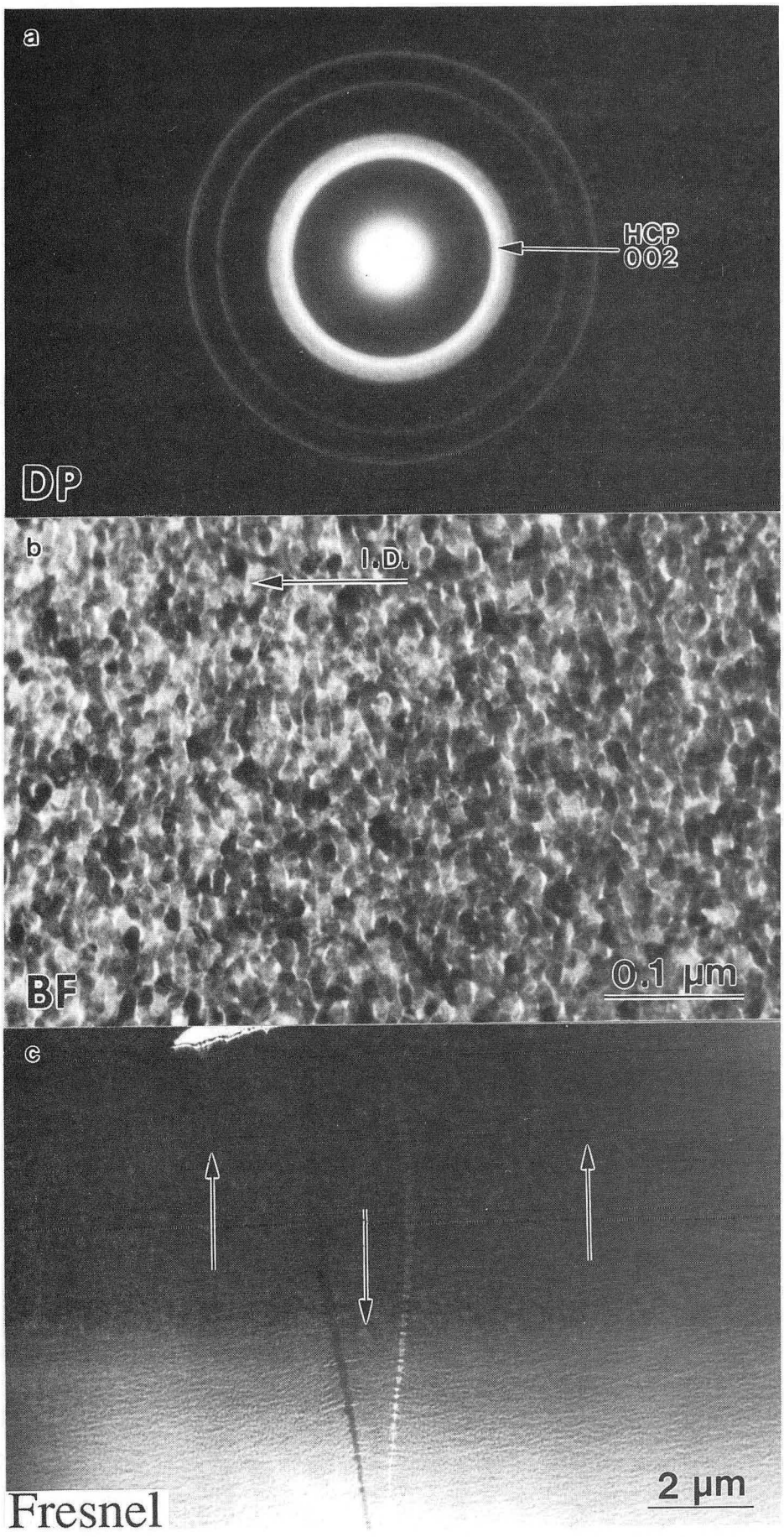

XBB8711-9462A

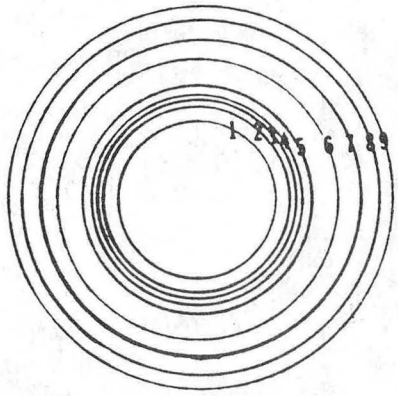

Ring No.	d-spacing (Å)	I/I_1 (HCP)	HCP Phase c = 4.06Å a = 2.50Å	FCC Phase a = 3.54Å	CoO(FCC) a = 4.26Å
1	2.46				111
2	2.17	20	$10\bar{1}0$		
3	2.03	60	0002	(111)	(200)
4	1.91	100	$10\bar{1}1$		
5	1.77			200	
6	1.51				220
7	1.25	80	$11\bar{2}0$		(311)
8	1.15	80	$10\bar{1}3$	(220)	
9	1.07	80	$11\bar{2}2$	(311)	

XBL 888-2772

XBB884-2852

XBB 8711-9463A

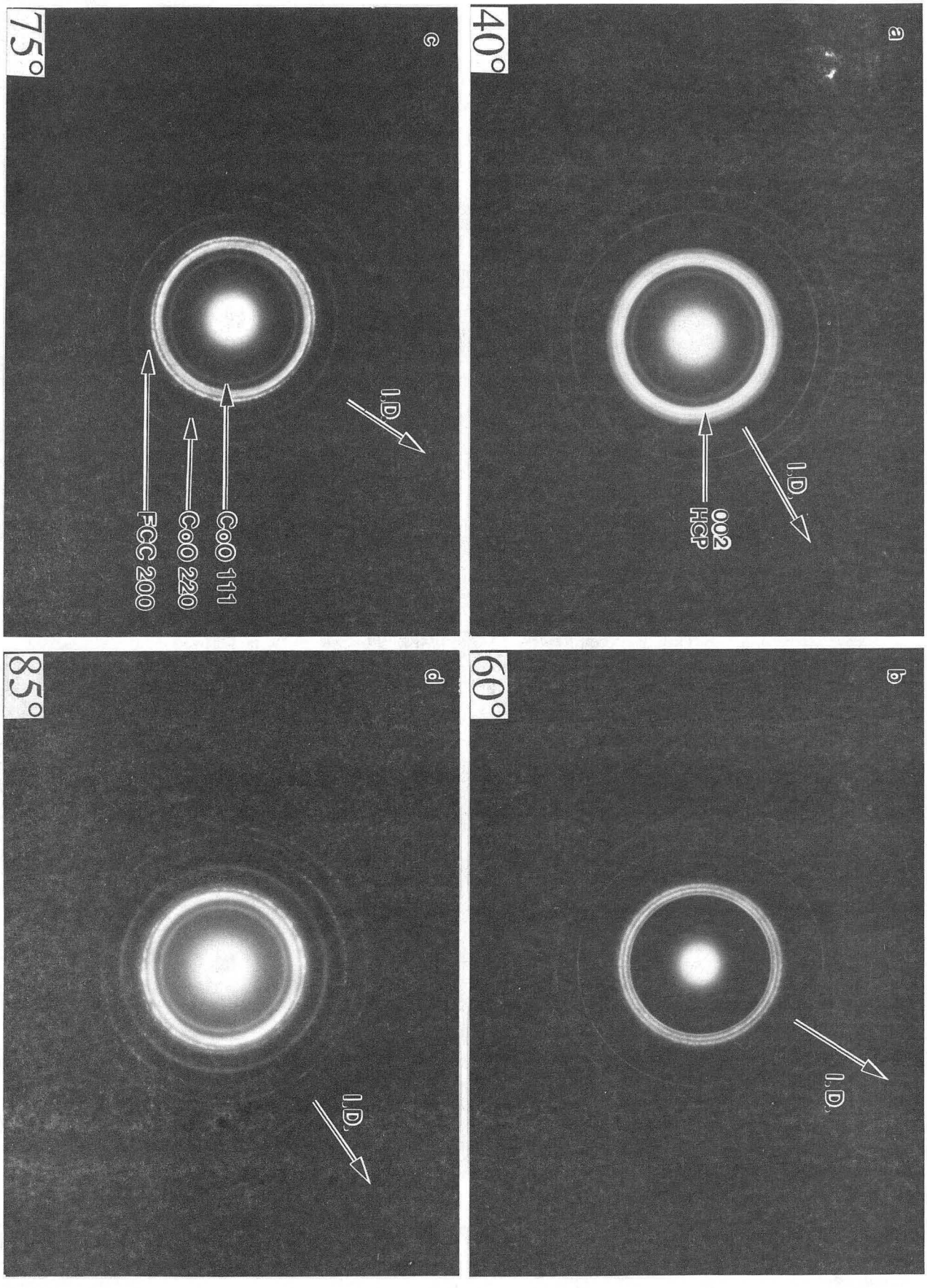

XBB 8710
8323A

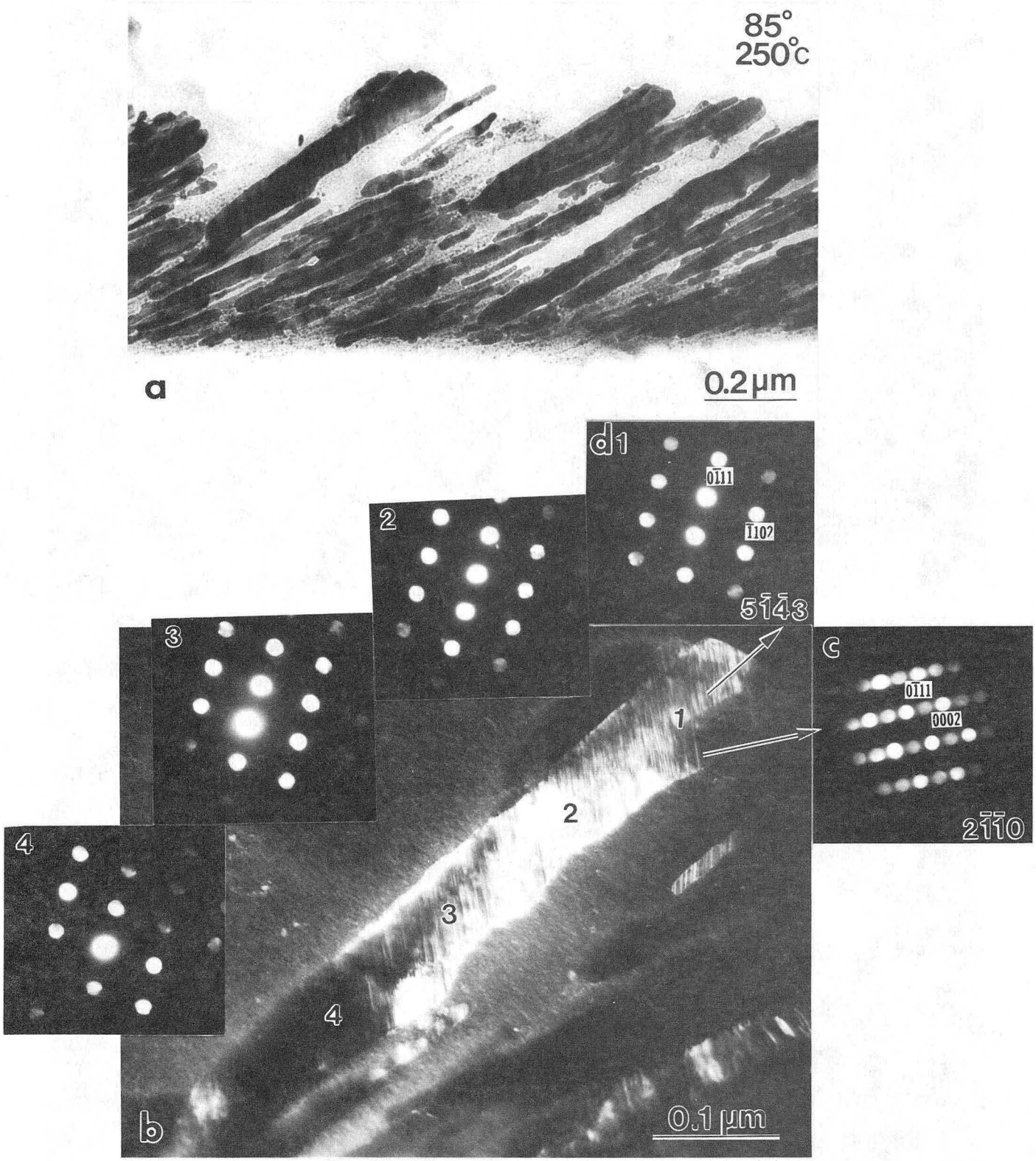
85°
250°C
a
0.2 μm
d1
0111
1102
5143
2
3
c
0111
0002
2110
1
2
3
4
4
b
0.1 μm

XBB 884-2853

LAWRENCE BERKELEY LABORATORY
TECHNICAL INFORMATION DEPARTMENT
UNIVERSITY OF CALIFORNIA
BERKELEY, CALIFORNIA 94720